PHYSICAL REVIEW B VOLUME 2, NUMBER 6 15 SEPTEMBER 1970

Electronic Transport in Alloys: Coherent-Potential Approximation*

K. Levin, B. Velický,† and H. Ehrenreich
Division of Engineering and Applied Physics, Harvard University, Cambridge, Massachusetts 02138
(Received 19 January 1970)

The coherent-potential approximation, which has been successfully used to describe the electronic structure of a nondilute binary alloy A_xB_{1-x}, is reformulated in a diagrammatic way suitable for the calculation of more complicated transport coefficients. This approach is applied to the calculation of three elementary transport coefficients: the conductivity σ, the thermoelectric power Q, and the low-field Hall coefficient R_H. The appropriate response functions are evaluated for a simple cubic tight-binding model. The rigid-band limit is considered in detail, with emphasis on the role of critical points. As the random alloy potential increases, deviations from rigid-band behavior – for example, Nordheim's rule – become more pronounced for unexpectedly small scattering strengths. However, the usual relations among the transport coefficients, e.g., Mott's equation between Q and σ, are maintained. The conductivity is no longer symmetrical with respect to electron and hole concentrations. Furthermore, the change in sign of Q and R_H may not occur when the band is half-full. Therefore, the identification of the carrier sign becomes ambiguous. For the model treated, numerical calculations are quite tractable. Examples are given which illustrate the behavior for a wide range of alloy parameters.

I. INTRODUCTION

The coherent potential approximation (CPA), which was originally formulated[1-3] to provide an approximate description of the equilibrium properties of nondilute random substitutional alloys A_xB_{1-x} having arbitrary concentrations and scattering strengths was recently extended[4,5] to apply to transport properties. In Ref. 4 attention was focused on the electrical conductivity which was calculated for a simple band model. The present paper extends these considerations to more general transport coefficients, the thermoelectric power, thermal conductivity, and Hall coefficient, and presents a diagrammatic way of calculating transport properties within the CPA. While this approach and that of Ref. 4 are identical for the case of the conductivity, the diagrammatic approach is to be preferred because it is easily applied to transport in the presence of an additional external field, e.g., the Hall coefficient. As in Refs. 3 and 5, we consider the band to have a simple cubic tight-binding structure. This will permit an investigation of the influence of critical points on transport properties and how this alters upon alloying.

The CPA is a self-consistent description, closely related to effective field theories formulated in connection with other physical problems and based on a single-site approximation. Independent electrons propagating in an effective crystalline medium, characterized by a complex self-energy $\Sigma(E)$, are scattered by randomly distributed atomic potentials measured relative to $\Sigma(E)$. The equilibrium properties are obtained from an approximate representation of the single-particle Green's function for the alloy derived using multiple-scattering theory. The response functions characterizing the transport coefficients are calculated by means of similar approximations for the two-particle Green's function, and, in the case of the Hall coefficient, for the three-particle Green's function.

The single-site approximation assumes that the total scattered wave in the medium is a sum of effective waves each coming from a single atom. Fluctuations in the effective wave coming from a particular atom in a given configuration are negligible when referred to the configuration averaged wave of that atom. This provides an equation for the self-energy in the CPA and motivates the two- and three-particle decoupling schemes which form the basis for an approximation of the transport coefficients.

In connection with both equilibrium and transport properties, the CPA is applicable to alloys of arbitrary concentrations and moderate scattering strengths. It produces correct results in the weak scattering and the dilute alloy limits and yields the third-order correction to the rigid-band calculation of the conductivity as well.[6] It is to be emphasized that it can be applied to alloy systems whose components have arbitrary band shape. However, it is restricted in its present form to short-range scattering potentials and to alloy components which have only a single band. As in Ref. 1, the electrons are assumed to interact only with the fixed atoms of the alloys. The effects of phonon scattering are neglected.

The paper is divided into five sections. In Sec.

II the macroscopic and microscopic transport coefficients are defined and the necessary apparatus needed to calculate the latter is discussed. We adopt a simple cubic tight-binding band model for the pure crystal and neglect the electron-electron interaction. The alloy is also assumed to be in a weak uniform magnetic field which is treated quasiclassically. The ingredients needed to calculate the microscopic coefficients are just the unperturbed alloy Hamiltonian in an external magnetic field and the perturbation terms which represent the effect of external electric fields and temperature gradients. Using time-dependent perturbation theory the transport coefficients are expressed in terms of single-particle correlation functions and the Kubo formulas[7] for the magnetic field-dependent (Hall) and field-independent conductivities at zero frequency and wave number are derived. It is shown that Mott's relation[8] between the conductivity and the thermoelectric power is obtained simply from the field-independent conductivity.

In Sec. III the approximate coefficients are defined as configuration averages of the exact transport coefficients evaluated in the CPA. A brief review of the single-particle CPA is given in Sec. III A. In Sec. III B a diagrammatic two-particle decoupling scheme consistent within the CPA is introduced, which reduces to that of Ref. 4, and in Sec. III C it is extended and applied to a three-particle decoupling. It is shown here that the approximations are consistent with such general properties of response functions as the Onsager relations. In Sec. IV a brief proof is given that the vertex corrections in the magnetic field-dependent and field-independent conductivities vanish. Physically this is equivalent to the statement that there is no back scattering within a Boltzmann equation context, and results from the assumption that the scattering is short range and therefore isotropic.

Finally, in Sec. V, easily evaluable expressions are given for the conductivity, the thermoelectric power, and the Hall coefficient. These are discussed and compared with the Boltzmann equation results. In Sec. V A the conductivity, thermoelectric power, and Hall coefficient are numerically calculated and displayed graphically as functions of Fermi energy E_F for fixed scattering strength δ and impurity concentration x at zero temperature. The rigid-band limit is discussed first, for comparative purposes, and the role of critical points in the pure crystal density of states is emphasized. It is seen that because of their dependence on the relaxation time $[(\mathrm{Im}\Sigma)^{-1}]$, the conductivity σ and thermoelectric power Q vary rapidly in the energy region around the critical points, whereas the Hall coefficient which depends primarily on $\mathrm{Re}\Sigma$ is not strongly affected by them. Variations in each of the three coefficients with increasing δ are then discussed. Here it is observed that for unexpectedly small δ, the rigid-band approximation is not valid. As δ is increased, the most striking behavior is seen in σ and Q; R_H as a function of E_F does not appreciably change with alloying. It is also evident that the signs of Q and R_H are not directly related except at the band edges.

In Sec. V B the x dependence of two transport coefficients σ and R_H for fixed electron concentration per atom is discussed. It follows from Mott's relation that Q can be obtained from $\sigma(x)$ and from the Fermi energy as a function of x. While this discussion is more pertinent to actually encountered experimental situations than that of Sec. V A, the results are more difficult to interpret because they depend on the variation of the Fermi energy with x. The weak scattering limits for the resistivity, $\rho = \sigma^{-1}$, i.e., the Nordheim $x(1-x)$ dependence, and for the Hall coefficient are considered first. As δ increases, significant departures from rigid-band behavior are apparent in both the resistivity and Hall coefficient as functions of x. These are displayed graphically for several values of the electron concentration per atom and for fixed δ. It is again seen from this discussion that the behavior of the resistivity is dependent on that of $\mathrm{Im}\Sigma$ while R_H depends primarily on $\mathrm{Re}\Sigma$.

II. TRANSPORT COEFFICIENTS

The exact linear phenomenological relations between induced macroscopic electrical and thermal currents, J and J^q, and external driving forces, in this case, an electric field E and temperature gradient ∇T are[9]

$$\vec{J} = L_{EE}\vec{E} + L_{ET}\nabla T \ , \tag{1a}$$

$$\vec{J}^q = L_{TE}\vec{E} + L_{TT}\nabla T \ . \tag{1b}$$

The L's are the transport coefficients; L_{EE} is the electric conductivity, $-L_{ET}/L_{EE}$ the thermoelectric power, L_{TE}/L_{EE} the Peltier coefficient, and $-L_{TT} + L_{TE}L_{ET}/L_{EE}$ the thermal conductivity. The coefficients are tensor quantities, in general. However, in a cubic crystal and in the absence of an external magnetic field, the thermoelectric power and the conductivity are scalars. If a weak magnetic field is then applied, the diagonal elements of L_{EE} to first order in the field H will be unchanged, but the off-diagonal elements will contain field-dependent terms. These off-diagonal elements of L_{EE} having both components transverse to the field play an important role in the Hall effect since the Hall field E_H is given in terms of the Hall coefficient R_H by

$$\vec{E}_H = R_H \vec{H} \times \vec{J} \,, \tag{2}$$

which involves current components perpendicular to the magnetic field. In the weak-field approximation, it can be shown[10] that if the field is in the $\hat{z}$ direction,

$$R_H = H^{-1} L_{EE}^{xy} / (L_{EE}^{xx})^2 \,. \tag{3}$$

For free electrons, using the Boltzmann equation R_H is given by $R_H = (nec)^{-1}$.

While the Hall coefficient is frequently used to determine the density and sign of the charge carriers, its interpretation is not entirely clear-cut for general band shapes when ne becomes a complicated function of the Fermi-surface geometry. The thermoelectric power also depends linearly on e, the electric charge. But because of its different dependence on band shapes and scattering mechanisms, the nature of the predicted charge carriers, as obtained from the sign of Q, may not agree with that of R_H.

The transport coefficients satisfy the Onsager relations[11]

$$L_{EE}^{ij}(H) = -L_{EE}^{ji}(H) \,, \tag{4a}$$

$$L_{EE}^{ij} = L_{EE}^{ji} \,, \tag{4b}$$

$$L_{ET} = -L_{TE}/T \,, \tag{4c}$$

which are consequences of time-reversal symmetry and independent of the nature of the system considered. In Eq. (4a), as throughout the paper, the field-dependent conductivity is assumed linear in H.

The system can be described microscopically by defining time- and space-dependent coefficients, for example, $L_{EE}(r, r'; t, t')$ where r and r', t and t' refer to the point and time at which J and E are measured, respectively. Analogous definitions can be made for other microscopic coefficients associated with L_{ET}, L_{TE}, and L_{TT}. Taking Fourier transforms of the microscopic coefficients leads to quantities $L(k, k'; \omega)$ which describe the wave number and frequency response of a system. This response is assumed to be translationally invariant in time but not necessarily in space.

The calculations of the microscopic coefficients are specified by the following assumptions about the alloy system:

(i) The alloy has a single band. In the pure crystal it is simple cubic tight binding, has width $2w$, and is characterized by an energy wave-number dispersion relation relative to its center given by[8]

$$W(k) = -\tfrac{1}{3} w(\cos ak_x + \cos ak_y + \cos ak_z) \,, \tag{5}$$

where a is the unit-cell dimension.

(ii) The Hamiltonian is given by[1]

$$\mathcal{H}^0 = \sum_n |n\rangle \epsilon_n \langle n| + \sum_{n \neq m} |n\rangle\, b_{nm} \langle m| \,, \tag{6}$$

$$\mathcal{H}^0 = V(R) + W(p) \,, \tag{7}$$

where $\epsilon_n = \epsilon^A$ or ϵ^B depending on whether an A or a B atom is at site n, and b_{nm} is assumed independent of alloy composition. $W(p)$ is the pure crystal Hamiltonian in which $\epsilon^A = \epsilon^B = 0$. R is the site coordinate. Such a model has the obvious shortcoming of assuming the "atomic energy levels" ϵ^A and ϵ^B to be independent of alloy composition, which, in general, is not the case. This particular model has been adopted here as well as in previous papers[1,3-5] to avoid complications.[12]

(iii) Only external fields which are slowly varying relative to the unit-cell dimensions will be considered. Consequently, the difficult questions which arise concerning the meaning of local thermal equilibrium of a system subjected to a nonuniform thermal gradient are avoided. Furthermore, the quasiclassical Hamiltonian

$$\mathcal{H} = W(\vec{p} - e\vec{A}^m/c) + V(R) \tag{8}$$

for the magnetic field may be used under these conditions. Here $\vec{A}^m$ is the vector potential corresponding to the magnetic field. $\vec{H} = H\hat{z}$ and R is regarded as a continuous variable.

$\vec{A}^m$ is written in the symmetric gauge at the outset as

$$\vec{A}^m = \tfrac{1}{2} \vec{H} \times \vec{R} \,. \tag{9}$$

The single-particle current operator is[7]

$$\vec{J} = e \nabla_p \mathcal{H} \tag{10a}$$

and is given to first order in H by

$$\vec{J} = e(\vec{v} - e\vec{A}^m \cdot \overleftrightarrow{M}^{-1}/c) \,, \tag{10b}$$

where the velocity and the components of the effective-mass tensor are, respectively, given by $v(k) = \nabla_k W(k)$ and $M_{ij}^{-1}(k) = \partial^2 W/\partial k_i \partial k_j$ in units for which $\hbar = 1$. In the case of a simple cubic tight-binding band Eq. (5), A^m and M^{-1} commute. For more complicated band models it would be necessary to include symmetrized terms in (10b). For the sake of simplicity, the discussion is limited to models for which the off-diagonal mass components vanish.

The magnetic interaction term in the weak-field case is

$$\mathcal{H}^m = -\vec{J} \cdot \vec{A}^m/c = -e\vec{v} \cdot \vec{A}^m/c \,. \tag{11}$$

Consequently, to first order in H, the Hamiltonian equation (8) may be written

$$\mathcal{H} \cong W(p) + V(R) + \mathcal{H}^m = \mathcal{H}^0 + \mathcal{H}^m \,. \tag{12}$$

The present discussion will always be limited to the weak-field approximation, and no powers in H higher than the first will be considered.

Additional terms must be added to $\mathcal{H}$ if an external electric field and temperature gradient are applied to the system. The effects of the electric

field are given by

$$\mathcal{H}^E(t) = -c^{-1}\int d^3R\,\vec{J}(R,t)\cdot\vec{A}^E(R,t)\,, \tag{13}$$

where $\vec{J}(R,t)$ is the single-particle current density operator in the interaction representation

$$\vec{J}(t) = e^{i\mathcal{H}t}\vec{J}(0)\,e^{-i\mathcal{H}t} \tag{14}$$

and

$$\frac{c^{-1}\partial\vec{A}^E}{\partial t} = \nabla\mathcal{V} \equiv -\vec{E}\ . \tag{15}$$

To describe the slowly varying thermal gradient ($\delta T/T \ll 1$), we introduce the following Hamiltonian:

$$\mathcal{H}^q(t) = -\int d^3R\,\vec{J}^q(R,t)\cdot\vec{A}^q(R,t)\quad, \tag{16}$$

where

$$e\vec{J}^q = \tfrac{1}{2}[\mathcal{H},\vec{J}]_+ - \mu\vec{J} \tag{17}$$

is the thermal current and μ is the chemical potential. In analogy with the electric vector potential

$$\frac{\partial\vec{A}^q}{\partial t} = \frac{\nabla T}{T}\ . \tag{18}$$

Although (16) differs from the usual form of the Hamiltonian describing thermal disturbances,[13] it is equivalent in the sense that all thermal transport coefficients derived from $\mathcal{H}^q$ are identical to those derived from the other Hamiltonian.

Using (13), it follows from time-dependent perturbation theory that the expectation value of the current at R and t induced by a weak external electromagnetic potential $\vec{A}^E$ is

$$\langle\vec{J}(R,t)\rangle_T = ic^{-1}\int d^3R'\int_{-\infty}^{t} dt'\,2\chi''_{JJ}(RR';t-t') \times\vec{A}^E(R',t') + \left\langle\frac{\partial\vec{J}}{\partial\vec{A}^E}\right\rangle\cdot\vec{A}^E(R,t)\,, \tag{19}$$

where the current response function

$$\chi''_{JJ}(RR';t-t') = \tfrac{1}{2}\mathrm{Tr}\rho(\mathcal{H})[J(R,t),\ J(R',t')] \tag{20}$$

$$\equiv \tfrac{1}{2}\langle[J(R,t),J(R',t')]\rangle_T \tag{21}$$

is a tensor quantity having ij elements χ''^{ij}_{JJ}. The brackets $\langle\ \rangle_T$ denote a thermal average and

$$\rho(\mathcal{H}) = [\exp\beta(\mathcal{H}-\mu)+1]^{-1} \tag{22}$$

is the single-particle density matrix, where $\beta = (k_BT)^{-1}$.

Identification of $\chi''_{JJ}(k,\omega)$ with $L_{EE}(k,\omega)$ is made possible by taking Fourier transforms. The problem of reducing a double Fourier transform containing two spatial coordinates to a single transform for small but finite wave vectors k may be circumvented in general along the lines summarized by Ehrenreich[14] by taking spatial averages of the response functions. However, the zero-wave-vector response functions may be obtained directly by integrating both sides of Eq. (19) over all R. It may be shown,[13] using the transform of a step function,

$$\eta(t-t') = \lim_{\epsilon\to 0}\frac{i}{2\pi}\int d\omega\,\frac{e^{-i\omega(t-t')}}{\omega+i\epsilon}\quad, \tag{23}$$

that

$$L^{ij}_{EE}(0,\omega) = \omega^{-1}\chi''^{ij}_{JJ}(0,\omega) + i\pi^{-1}\mathcal{P} \times\int_{-\infty}^{\infty} d\omega'\,\chi''^{ij}_{JJ}(0,\omega)[(\omega-\omega')\omega']^{-1}, \tag{24a}$$

Similarly,

$$-TL_{ET}(0,\omega) = \omega^{-1}\chi''_{JJ^q}(0,\omega) + i\pi^{-1}\mathcal{P} \times\int_{-\infty}^{\infty} d\omega'\,\chi''_{JJ^q}(0,\omega')[(\omega-\omega')\omega']^{-1}\ , \tag{24b}$$

where χ''_{JJ^q} is given by Eq. (21) with the second J replaced by J^q. The Cartesian indices on χ''_{JJ^q} have been omitted because we are interested only in its diagonal elements (H independent) which are the only ones that appear in a cubic crystal. In the same way L_{TT} and L_{TE} may be calculated by defining the appropriate response function χ'' and using the perturbation Hamiltonians discussed above.

As a consequence of their analyticity in a half-plane, the response functions can be shown to satisfy properties which are listed in Appendix A. Using these properties we may conclude that for static ($\omega = 0$) responses which are of interest here, the imaginary contributions to L_{EE} and L_{ET} will vanish. Thus,

$$L^{ij}_{EE}(0,0) = \omega^{-1}\chi''^{ij}_{JJ}(0,\omega)\big|_{\omega=0}, \tag{25a}$$

$$-TL_{ET}(0,0) = \omega^{-1}\chi''_{JJ^q}(0,\omega)\big|_{\omega=0}\,, \tag{25b}$$

$$L^{ij}_{EE}(0,0;H) = -i\pi^{-1}\mathcal{P} \times\int_{-\infty}^{\infty} d\omega'\,\chi''^{ij}_{JJ}(0,\omega';H)/\omega'^2\,. \tag{25c}$$

The arguments H in Eq. (25c) refer to the fact that these quantities depend linearly on the magnetic field H.

The Onsager relations may be verified for the microscopic coefficients $L_{EE}(0,\omega)$ and $L_{ET}(0,\omega)$ using the results in Appendix A. Because

$$\chi''^{ij}_{JJ}(0,\omega) = \chi''^{ji}_{JJ}(0,\omega)\,, \tag{A5}$$

$$\chi''^{ij}_{JJ}(0,\omega;H) = -\chi''^{ji}_{JJ}(0,\omega;H)\,, \tag{A6}$$

and in analogy with (25b),

$$L_{TE}(0,0) = \omega^{-1}\chi''_{J^qJ}(0,\omega)\big|_{\omega=0}\,, \tag{26}$$

it follows that

$$L^{ij}_{EE}(0,0;H) = -L^{ji}_{EE}(0,0;H)\,, \tag{27a}$$

$$L^{ij}_{EE}(0,0) = L^{ji}_{EE}(0,0)\,, \tag{27b}$$

and

$$L_{ET}(0,0) = -L_{TE}(0,0)/T\,, \tag{27c}$$

which are identical with Eqs. (4).

The macroscopically observable quantities correspond not to the transport coefficients for a given alloy configuration, but to the configuration-averaged coefficients $\langle L\rangle$. To calculate these quantities it is convenient to separate thermodynamic and configuration averages. This simplification can be made by use of the identity

$$\rho(\mathcal{H}) = \int d\eta\, \rho(\eta)\delta(\eta - \mathcal{H})\,. \tag{28}$$

From Eqs. (20) and (25a), we then obtain for the configuration-averaged conductivity

$$\langle L_{EE}^{ij}(0,0)\rangle = \tfrac{1}{2}\lim_{\omega\to 0}\int\int d\eta\, dt\, e^{i\omega(t-t')} \times \omega^{-1}\,\mathrm{Tr}\rho(\eta)\langle\delta(\eta-\mathcal{H})[J_i(t), J_j(t')]\rangle. \tag{29}$$

The temperature-dependent factor $\rho(\eta)$ is thereby seen to be separated from the configuration-averaged quantity appearing in the brackets on the right-hand side of Eq. (29). From now on we shall drop the arguments in $\langle L_{EE}^{ij}(0,0)\rangle$ and write simply $\langle L_{EE}^{ij}\rangle$. Performing the t integration and evaluating the limit yields for the field-independent conductivity

$$\langle L_{EE}^{ij}\rangle = -\pi\int d\eta\rho'(\eta)\,\mathrm{Tr} e v_i\langle\delta(\eta-\mathcal{H}^0)\, e v_j\delta(\eta-\mathcal{H}^0)\rangle. \tag{30}$$

Similarly, one obtains,

$$T\langle L_{ET}\rangle = \pi e^{-1}\Big[\int d\eta\rho'(\eta)\eta\,\mathrm{Tr} e v_i\langle\delta(\eta-\mathcal{H}^0) \times e v_i\,\delta(\eta-\mathcal{H}^0)\rangle - \mu\langle L_{EE}^{ij}\rangle\Big]\,, \tag{31}$$

and the field-dependent conductivity is given by

$$\langle L_{EE}^{ij}(H)\rangle = -i\mathcal{P}\int\int d\eta\, d\omega'\omega'^{-2}[\rho(\eta)-\rho(\eta+\omega')] \times \mathrm{Tr} J_i\langle\delta(\eta+\omega'-\mathcal{H})J_j\,\delta(\eta-\mathcal{H})\rangle. \tag{32}$$

Because the first two expressions are field independent, they contain the Hamiltonian $\mathcal{H}^0$ in Eq. (7). The last expression contains the field-dependent Hamiltonian $\mathcal{H}$ of Eq. (12) and the field-dependent current operators (10b). Equations (30)–(32) are just the configuration-averaged Kubo-Greenwood formulas.[7]

At this stage it is possible to eliminate $\langle L_{ET}\rangle$ completely and to solve for the thermopower Q in terms of $\langle L_{EE}\rangle$. Using the low-temperature expansion of the single-electron density matrix ρ, one may conclude that, for small T,

$$Q = -\frac{\langle L_{ET}\rangle}{\langle L_{EE}^{ii}\rangle} = \frac{\pi^2}{3e}\,\frac{k_B^2 T\, d\ln\langle L_{EE}^{ii}\rangle}{dE_F}\,, \tag{33}$$

where k_B is Boltzmann's constant, E_F is the Fermi energy, and T is the absolute temperature. This equation is sometimes referred to as Mott's rule.[8] This simple result derives from the application of Eq. (28) which makes it possible to separate thermodynamic and configuration averages.

Mott's relation is an exact result for noninteracting electrons independent of the details of the system considered. It should be emphasized that the weak scattering assumptions which are ordinarily used in its derivation are not necessary, nor are any of the assumptions made earlier concerning a specific band shape.

Except for the single-particle picture, no approximations have been made up to now. The disordered system has been treated exactly. However, Eqs. (30)–(32) are very difficult to handle because of their dependence on the complicated random alloy Hamiltonian. To evaluate the averaged coefficients explicitly, we need to consider

$$\langle\delta(\eta-\mathcal{H})J_i\,\delta(\eta-\mathcal{H})\rangle\,, \tag{34}$$

which contains all of the dependence of the $\langle L\rangle$'s on the random Hamiltonian. However, because this average is difficult to perform exactly, it is the purpose of Secs. III and IV to evaluate (34) approximately. The remainder of this section is devoted to rewriting Eqs. (30)–(32) in a form suitable for approximation. We introduce the magnetic field-dependent and field-independent Green's functions

$$G(H,z) = (z-\mathcal{H})^{-1} \tag{35}$$

and

$$G(z) = (z-\mathcal{H}^0)^{-1}\,, \tag{36}$$

where $\mathcal{H}=\mathcal{H}^0+\mathcal{H}^m$ is the Hamiltonian for the alloy in a magnetic field. To first order in the field

$$G(H,z) \cong G(z) + G(z)\mathcal{H}^m G(z)\,. \tag{37}$$

By defining

$$z_i = \eta + is\lambda_i\,, \tag{38}$$

where $\lambda_i = \pm 1$, $i = 1, 2, 3$ and s is an arbitrarily small positive number, we may write Eqs. (30)–(32), using Eqs. (35)–(37) as

$$\langle L_{EE}^{ij}\rangle = (4\pi)^{-1}\int d\eta\rho'(\eta) \times \sum_{\lambda_1\lambda_2} I^{(2)}(ev_i, ev_j; z_1, z_2)(-1)^{(\lambda_1-\lambda_2)/2} \tag{39a}$$

and

$$\langle L_{EE}^{ij}(H)\rangle = i(2\pi)^{-2}\mathcal{P}\int d\eta\, d\omega'(\omega')^{-2}\Big\{[\rho(\eta)-\rho(\eta+\omega')] \times \sum_{\lambda_1\lambda_2}(-1)^{(\lambda_1-\lambda_2)/2}\Big[I^{(2)}\Big(\frac{ev_i - e^2A_i^m M_{ji}^{-1}}{c}; z_1+\omega', z_2\Big) + I^{(2)}(-e^2A_i^m M_{ii}^{-1}/c, ev_j; z_1+\omega', z_2) + I^{(3)} \times (ev_i, ev_j, \mathcal{H}^m; z_1+\omega', z_2, z_2)$$

$$+I^{(3)}(ev_i, \mathcal{H}^m, ev_j; z_1+\omega', z_1+\omega', z_2)\Big]\Big\}, \quad (39b)$$

where

$$I^{(2)}(C_1, C_2; z_1, z_2) = \mathrm{Tr} C_1 \langle G(z_1) C_2 G(z_2)\rangle \quad (40a)$$

and

$$I^{(3)}(C_1, C_2, C_3; z_1, z_2, z_3) = \mathrm{Tr} C_1 \langle G(z_1) C_2 G(z_2) C_3 G(z_3)\rangle . \quad (40b)$$

To derive Eq. (39b), all of the linear terms in H in (32) have been explicitly extracted from J and $G(z, H)$.

III. DECOUPLING SCHEMES IN CPA

It is the purpose of this section to develop an approximation scheme for evaluating $I^{(2)}$ and $I^{(3)}$.[15] The discussion will be divided into three parts in order of increasing complexity. First, the CPA will be applied to the one-particle Green's function $G(z)$ so that the propagation of a single particle may be understood. Next, it will be applied to $I^{(2)}$ which is related to a two-particle Green's function, and, finally to $I^{(3)}$ which is related to a three-particle Green's function. Section III A will briefly summarize recent work[1,3]; Sec. III B will introduce a diagrammatic technique for obtaining $I^{(2)}$ which leads to the same expression as was found by an analytic, rather than diagrammatic, technique in Ref. 4. Section III C will use the diagrammatic approach to calculate $I^{(3)}$, which previously has not been considered. While this last calculation would be difficult if performed along the lines of Ref. 4, the diagrams for $I^{(3)}$ provide a more tractable framework.

A. Single-Particle CPA

The quantity we wish to determine first for the alloy is

$$\langle G(z)\rangle \equiv \overline{G}(z) = [z - W - \Sigma(z)]^{-1} \quad (41)$$

the configuration average of the single-electron Green's function. Here the operator W is the second term on the right-hand side in Eq. (6). $\overline{G}$ has the crystal translational symmetry. Σ is the self-energy operator which for the short-range model Hamiltonian [Eq. (6)] depends only on z and is independent of k.

The T matrix for the electrons is defined by

$$G(z) = \overline{G}(z) + \overline{G}(z)\, T(z)\, \overline{G}(z) . \quad (42a)$$

Since

$$\langle G(z)\rangle = \overline{G} ,$$

$$\langle T(z)\rangle = 0 . \quad (42b)$$

This is a self-consistent equation for determining $\overline{G}$. The CPA consists of applying to Eq. (42b) a single-site decoupling. From multiple-scattering theory, T may be written as a sum of single-site contributions,

$$T = \sum_n T_n + \sum_{n\neq m} T_n \overline{G}\, T_m + \sum_{n\neq m, m\neq l} T_n \overline{G}\, T_m \overline{G}\, T_l + \cdots , \quad (43)$$

where

$$T_n = [\,|n\rangle (\epsilon_n - \Sigma_n)\langle n|\,](1 + \overline{G}\, T_n) \quad (44)$$

and

$$\Sigma_n(z) = \langle n|\Sigma(z)|n\rangle \quad (45)$$

for the Hamiltonian in Eq. (6). The single-site approximation for $\langle T\rangle$ consists in averaging independently each individual scattering event,

$$\langle T\rangle = \sum_{n\neq m, m\neq l} \langle T_n\rangle (1 + \overline{G}\langle T_m\rangle + \overline{G}\langle T_m\rangle\, \overline{G}\langle T_l\rangle + \cdots). \quad (46)$$

Equation (42b) then leads to the condition

$$\langle T_n\rangle = 0 . \quad (47)$$

Writing

$$T_n(z) = |n\rangle\, t_n(z)\langle n| , \quad (48a)$$

we find from Eq. (44) that

$$t_n(z) = [\epsilon_n - \Sigma(z)]\{1 - [\epsilon_n - \Sigma(z)]\langle n|\,\overline{G}\,|n\rangle\}^{-1}, \quad (48b)$$

and from (47),

$$\Sigma(z) = \epsilon + xy\delta^2 F[z - \Sigma(z)]\{1 + [\epsilon + \Sigma(z)]F[z - \Sigma(z)]\}^{-1}, \quad (49)$$

where we have dropped the subscript n on $\Sigma_n(z)$ and written simply $\Sigma(z)$. Since the self-energy is a multiple of the unit operator, $\Sigma_n(z)$ is independent of n. In Eq. (49) $y = 1 - x$, $\delta = (\epsilon^A - \epsilon^B)/2w$, $F(z) = \langle n|\overline{G}|n\rangle$, and $\epsilon = x\epsilon^A + y\epsilon^B$ is the average "atomic" energy level of the alloy. The energy origin is chosen so that $\epsilon^A = \frac{1}{2}\delta$, $\epsilon^B = -\epsilon^A$, and $w = 1$, so that the bandwidth is 2. Equation (49) implies that only three parameters are necessary to determine the self-energy in the CPA. These are x the concentration of impurities, δ the scattering strength parameter, and $g(E) = -\pi^{-1}\,\mathrm{Im}F(E)$ the density of states in the pure crystal.

B. Evaluation of $I^{(2)}$

In transport phenomena, the correlated motion of several particles or particles and holes must be taken into account. The expressions appearing in the transport coefficients involve configuration-averaged products of two Green's functions for the field-independent conductivity and three Green's functions for the field-dependent conductivity.

We shall now evaluate $I^{(2)}(C_1, C_2; z_1, z_2)$ analytically as was done in Ref. 4 using a decoupling suggested by the single-particle decoupling in Eq. (46). This will be followed by the introduction of a dia-

grammatic representation of $I^{(2)}$. A detailed discussion of its analytic properties can be found in Ref 4. Comparing the diagrams and the explicit expression for $I^{(2)}$ will yield a set of diagrammatic rules physically consistent with the single-site approximation in multiple-scattering theory. These rules are then used as a starting point for the calculation of $I^{(3)}$.

We first make the substitution $G=\overline{G}+\overline{G}T\overline{G}$ in Eq. (40a). Then[16]

$$I^{(2)}(C_1, C_2; z_1, z_2)=\mathrm{Tr}C_1\overline{G}(z_1)\,C_2\overline{G}(z_2)$$
$$+\mathrm{Tr}C_1\overline{G}(z_1)\langle T(z_1)\,\overline{G}(z_1)C_2\overline{G}(z_2)T(z_2)\rangle\,\overline{G}(z_2). \quad (50)$$

In order to evaluate Eq. (50), we use (43) and apply a decoupling consistent with the single-site approximation in (46). The results of this decoupling are

$$\mathrm{Tr}C_1\overline{G}\langle T\overline{G}C_2\overline{G}T\rangle\,\overline{G}=\mathrm{Tr}C_1\overline{G}\,\sum_n\langle T_n\overline{G}C_2\overline{G}T_n\rangle\overline{G}$$
$$+\mathrm{Tr}C_1\,\overline{G}\sum_{n\neq m}\langle T_n\overline{G}\langle T_m\overline{G}C_2\overline{G}T_m\rangle\overline{G}T_n\rangle\,\overline{G}+\cdots, \quad (51a)$$

where we average over each *pair* of scattering events separately. It is thus seen that the motion of two particles in the medium is correlated only if they both scatter from the same site. The consistency of this factorization with the CPA to the single-particle Green's function may be verified[4] by demonstrating the existence of a type of Wards identity which relates $I^{(2)}$ and Σ. In addition, various identities involving the approximate linear response function $\langle\chi\rangle$ (see Appendix A) may be shown to be satisfied so that this two-particle decoupling appears to be physically reasonable. These identities will be discussed shortly in connection with $I^{(3)}$.

We define the vertex operator $\Gamma^{(2)}$ by

$$I^{(2)}(C_1, C_2; z_1, z_2)=\mathrm{Tr}C_1\overline{G}C_2\overline{G}+\mathrm{Tr}C_1\overline{G}\Gamma^{(2)}(C_2)\overline{G}\,, \quad (51b)$$

where

$$\Gamma^{(2)}(C_2)=\langle T\overline{G}C_2\overline{G}T\rangle\,. \quad (51c)$$

It follows from Eq. (51a) that

$$\Gamma^{(2)}=\sum_n\Gamma_n^{(2)}\,, \quad (52a)$$

where

$$\Gamma_n^{(2)}=\langle T_n\overline{G}C_2\overline{G}T_n\rangle+\sum_{m\neq n}\langle T_n\overline{G}\langle T_m\overline{G}C_2\overline{G}T_m\rangle\overline{G}T_n\rangle+\cdots. \quad (52b)$$

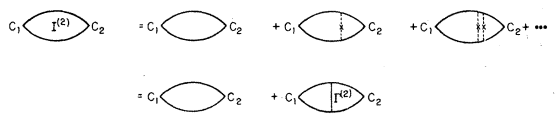

FIG. 1. Diagrammatic representation of the decoupled form of $I^{(2)}$ [Eq. (50)]. The second equation defines $\Gamma^{(2)}$ the vertex corrections for two particles.

$\Gamma^{(2)}$ may thus be written as a sum of single-site contributions.

Equations (51) may be combined and written diagrammatically as in Fig. 1. The diagrammatic expression for $\Gamma^{(2)}$ is also shown. The first line in the figure illustrates the sequence of scattering events which contribute to $I^{(2)}$. The first term on the right-hand side is the first term in (50); the second represents two particles scattering at a single site and the third, two particles scattering at two sites which are different from one another. These last two terms are written analytically in Eq. (51a). The infinite series of diagrams is summed diagrammatically in the second line in the figure in terms of the vertex corrections $\Gamma^{(2)}$ defined in (51b). Solid lines are to be associated with the average propagator $\overline{G}$ and dotted lines with two particles scattering from a single site denoted by a cross.

The rules for obtaining this diagrammatic decoupling are the following:

(i) No crossed dotted lines are allowed. This is equivalent to the neglect of clusters.

(ii) Two adjacent unconnected dotted lines always refer to different sites. This reflects the fact, expressed mathematically in Eq. (43), that the particle is never allowed to scatter twice in succession at the same site.

(iii) All disconnected dotted lines are averaged over separately. These three rules represent a two-particle decoupling which is a natural generalization of the single-particle decoupling, expressed in Eq. (46).

C. Evaluation of $I^{(3)}$

With the rules given in Sec. III B, we now have a simple means of obtaining $I^{(3)}$. Substituting $G=\overline{G}+\overline{G}T\overline{G}$ into (40b), where $\overline{G}$ is defined in (41) and using the fact that $\langle T\rangle=0$, one finds that

$$I^{(3)}(C_1, C_2, C_3; z_1, z_2, z_3)=\mathrm{Tr}C_1\overline{G}C_2\overline{G}C_3\overline{G}+\mathrm{Tr}C_1\overline{G}\langle T\overline{G}C_2\overline{G}T\rangle\,\overline{G}C_3\overline{G}+\mathrm{Tr}C_1\overline{G}C_2\overline{G}\,\langle T\overline{G}C_3\overline{G}T\rangle\,\overline{G}$$
$$+\mathrm{Tr}C_1\overline{G}\langle T\overline{G}C_2\overline{G}C_3\overline{G}T\rangle\,\overline{G}+\mathrm{Tr}C_1\overline{G}\langle T\overline{G}C_2\overline{G}T\overline{G}C_3\overline{G}T\rangle\,\overline{G}\,. \quad (53)$$

All the terms in Eq. (53) but the last can be evaluated according to the two-particle decoupling scheme discussed in Sec. III B because they involve processes in which two particles are coupled while

the third propagates independently. The corresponding diagrams can be written down at once. For example, the second term on the right-hand side which involves a factorization of a product of two propagators may be written diagrammatically as in Fig. 2(a). The vertex at C_2 corresponds to $\Gamma^{(2)}(C_2)$, defined analytically in Eq. (51c) and diagrammatically in Fig. 1.

In the last term in (53), which involves three T matrixes, the motion of all three particles is coupled. Some diagrams contributing to this last expression in (53) are shown in Figs. 2(b) and 2(c). The corresponding analytical expressions for each of the diagrams in Figs. 2(a)–2(c) are as follows:

$$\text{Fig. 2(a)} = \sum_n \mathrm{Tr} C_1 \overline{G} \Gamma_n^{(2)}(C_2) \overline{G} C_3 \overline{G} \,, \tag{54a}$$

$$\text{Fig. 2(b)} = \sum_{n \neq m} \mathrm{Tr} C_1 \overline{G} \langle T_n \overline{G} C_2 \overline{G} T_n \rangle \overline{G} \langle T_m \overline{G} C_3 \overline{G} T_m \rangle \overline{G}$$
$$+ \sum_{n \neq m, m \neq l} \mathrm{Tr} C_1 \overline{G} \langle T_n \overline{G} C_2 \overline{G} T_n \rangle \overline{G} \langle T_m \overline{G} \langle T_l \overline{G} C_3 \overline{G} T_l \rangle \overline{G} T_m \rangle \overline{G} + \cdots$$
$$= \sum_{n \neq m} \mathrm{Tr} C_1 \overline{G} \Gamma_n^{(2)}(C_2) \overline{G} \Gamma_m^{(2)}(C_3) \overline{G} \,, \tag{54b}$$

and

$$\text{Fig. 2(c)} = \sum_{n \neq m} \mathrm{Tr} C_1 \overline{G} \langle T_n \overline{G} \Gamma_m^{(2)}(C_2) \overline{G} T_n \overline{G} C_3 \overline{G} T_n \rangle \overline{G} \,, \tag{54c}$$

where $\Gamma_n^{(2)}$ is defined in Eq. (52a). For the term represented by Fig. 2(b) some individual diagrams as well as the sum of the infinite series corresponding to this term are shown. This diagrammatic equation represents Eq. (54b). The dotted line having a Y shape in Fig. 2(c) corresponds to three particles scattering at a given site and, thus, involves three factors T_n. It is clear from this last example that the diagrammatic rules must be extended to include dotted lines having a Y shape as well as simple dotted lines. From the rules, it follows that they must not cross (hence, there can be at most one dotted Y), and they are averaged separately from all other dotted lines.

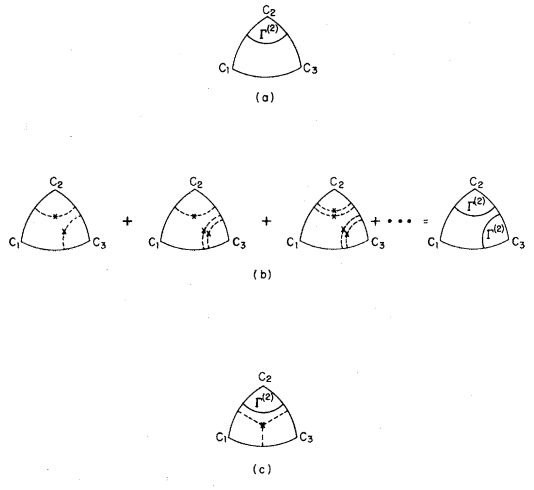

FIG. 2. Some diagrams contributing to $I^{(3)}$ [see Eqs. (54)].

Fig. 3(a) shows the complete diagrammatic expression for $I^{(3)}$ given by Eq. (53) in decoupled form. This includes the three diagrams in Fig. 2. These three examples [see Eqs. (54a)–(54c)] show how analytical expressions in terms of T_n and $\Gamma_n^{(2)}$ may be determined for all the diagrams in $I^{(3)}$. For this reason, as well as the fact that there are a large number of contributing terms, the complete analytic expression for $I^{(3)}$ will be omitted here.

It is convenient, finally, to introduce the vertex corrections corresponding to $I^{(3)}$, defined in analogy with Eq. (51b),[17]

$$I^{(3)}(C_1, C_2, C_3; z_1, z_2, z_3)$$
$$= \mathrm{Tr} C_1 \overline{G} C_2 \overline{G} C_3 \overline{G} + \mathrm{Tr} C_1 \overline{G} \Gamma^{(3)}(C_2, C_3) \overline{G} \,. \tag{55}$$

Diagrammatically, this may be written as shown in Fig. 3(b). Fig. 3 may be given the following simple interpretation. The vertex corrections $\Gamma^{(3)}$ are composed of "pair-wise correlations" [represented by $\Gamma^{(2)}(C_i)$, $i = 1-3$, where i can be associated with the pair of particles whose propagator lines intersect at C_i] as well as correlations between the entire triplet of particles (represented by a dotted Y). These correlations in a single-site approximation occur only if the pair or the triplet of particles scatters from the same site.

We shall now verify that the three-particle decoupling scheme introduced here is consistent with the known analytic behavior of the field-dependent correlation function defined by

$$\langle\chi(C_1, C_2, z; C_3)\rangle = (2\pi i)^{-2}\int\{d\eta\, dz'[\rho(\eta)-\rho(\eta+z')](z'-z)^{-1}\sum_{\lambda_1\lambda_2}(-1)^{(\lambda_1-\lambda_2)/2}$$

$$\times[I^{(3)}(C_1, C_3, C_2;\ z_1+z', z_1+z', z_2)+I^{(3)}(C_1, C_2, C_3;\ z_1+z', z_2, z_2)]\}\ , \tag{56}$$

where λ_1, λ_2, z_1, z_2 are the variables defined in Eq. (38). This expression is obtained using the response function χ'' defined in Eq. (21), and expanding to first order in the external field C_3. Equations (A1) and (A2) express $\chi(z)$ in terms of $\chi''(z)$. It is assumed for simplicity that C_1 and C_2 are independent of C_3. The four properties of the field dependent χ that we wish to verify are

(i) $\langle\chi(C_1, C_2; -z^*; C_3)\rangle^* = \langle\chi(C_1, C_2; z; C_3)\rangle$; (57a)

(ii) $\langle\chi(\mathcal{O}C, \mathcal{O}^\dagger, \mathcal{O}C_2\mathcal{O}^\dagger; z; \mathcal{O}C_3\mathcal{O}^\dagger)\rangle$

$$= \langle\chi(C_1, C_2; z;\ C_3)\rangle\ , \tag{57b}$$

where $\mathcal{O}$ is a translation operator belonging to the crystal symmetry group.

(iii) The Onsager relation

$$\langle L_{EE}^{ij}(0, 0; H)\rangle = -\langle L_{EE}^{ij}(0, 0; H)\rangle$$

is obeyed;

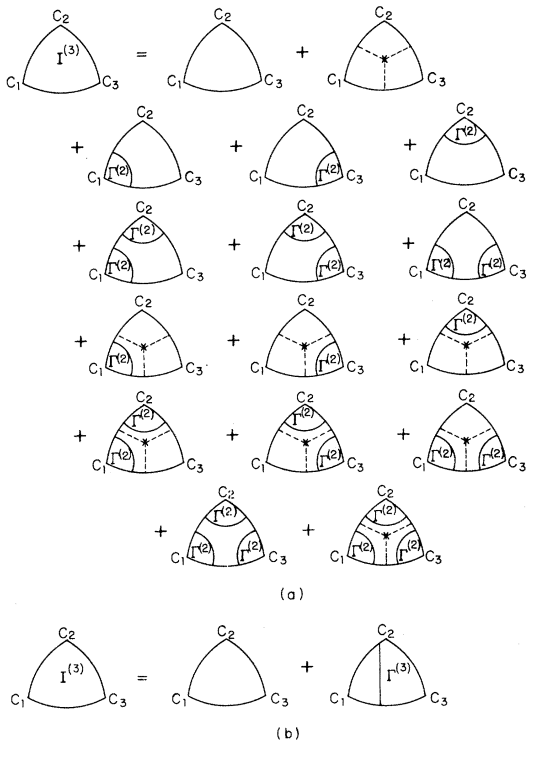

FIG. 3. Diagrammatic representation of the complete decoupled form of $I^{(3)}$ [Eq. (53)]. Figure 3(b) defines the three-particle vertex corrections $\Gamma^{(3)}$.

(iv) $\lim_{z\to\infty}\langle\chi(C_1, C_2; z; C_3)\rangle = z^{-1}\langle\mathrm{Tr}[C_1, C_2]\rho(\mathcal{K})\rangle$, (57c)

where $\mathcal{K}=\mathcal{K}^0+C_3$ is the field-dependent Hamiltonian and C_3 is treated linearly. Comparing Eqs. (57) with (A7)–(A9) in Appendix A, it is seen that the quantities $\chi(C_1, C_2; z)$ satisfy the same identities as $\langle\chi(C_1, C_2; z; C_3)\rangle$. While the external field C_3 is treated linearly in $\langle\chi(C_1, C_2; z; C_3\rangle$, the identities (A7)–(A9) in fact are valid to all orders in C_3. It follows from (i)–(iv) that $I^{(3)}$ should obey the following relations if the approximation is to be physically reasonable:

$$[I^{(3)}(C_1, C_2, C_3; z_1, z_2, z_3)]^*$$

$$= I^{(3)}(C_1, C_3, C_2; z_3^*, z_2^*, z_1^*)\ , \tag{58a}$$

$$I^{(3)}(\mathcal{O}C_1\mathcal{O}^\dagger, \mathcal{O}C_2\mathcal{O}^\dagger, \mathcal{O}C_3\mathcal{O}^\dagger; z_1, z_2, z_3)$$

$$= I^{(3)}(C_1, C_2, C_3; z_1, z_2, z_3)\ , \tag{58b}$$

$$I^{(3)}(C_1, C_2, C_3; z_1, z_2, z_3) = I^{(3)}(C_3, C_1, C_2; z_3, z_1, z_2)$$

$$= I^{(3)}(C_2, C_3, C_1; z_2, z_3, z_1)\ , \tag{58c}$$

and

$$\lim_{z\to\infty} I^{(3)}(C_1, C_2, C_3; z_1, z_2, z_3)$$

$$= (z_1)^{-1}\,\mathrm{Tr}C_1C_2\langle G(z_2)C_3G(z_3)\rangle\ . \tag{58d}$$

As shown in Ref. 4, analogous identities hold for $I^{(2)}$ as well.

The first three identities may be verified term by term by writing each term in $I^{(3)}$ in terms of the T_n and performing the averages explicitly, making use of the identity

$$\langle T_n\rangle = xT_n^A + yT_n^B\ , \tag{59}$$

where T_n^A is given by (44) with $\epsilon_n=\epsilon^A$. To prove (58d) requires an extra argument: as $z\to\infty$, $\overline{G}\sim z^{-1}$ and, from Eq. (49), $\Sigma(z)\sim\epsilon$; therefore, $T_n(z)\sim z^0$. Then, the only terms which contribute to the left-hand side of (58d) are those in which $\overline{G}(z_1)$ appears linearly. Therefore, it follows that

$$\lim_{z_1\to\infty} I^{(3)}(C_1, C_2, C_3; z_1, z_2, z_3)$$

$$= (z_1)^{-1}\,\mathrm{Tr}C_1C_2\overline{G}(z_2)C_3\overline{G}(z_3)$$

$$+ (z_1)^{-1}\,\mathrm{Tr}C_1C_2\overline{G}(z_2)\langle T(z_2)\overline{G}(z_2)C_3\overline{G}(z_3)T(z_3)\rangle\overline{G}(z_3) \tag{60a}$$

$$= (z_1)^{-1}\,\mathrm{Tr}C_1C_2\langle G(z_2)C_3G(z_3)\rangle\ , \tag{60b}$$

which proves (58d). This last relation is of parti-

cular interest because it demonstrates a consistency of the two- and three-particle decoupling schemes.

IV. VANISHING OF CONDUCTIVITY VERTEX CORRECTIONS

We now specialize to the three operators C_1, C_2, and C_3 which appear as arguments of $I^{(2)}$ and $I^{(3)}$ in Eqs. (39a) and (39b). It is important to note in the case of $I^{(2)}(C_1, C_2; z_1, z_2)$ at least one of the operators C_i, will be a velocity operator v. In the case $I^{(3)}(C_1, C_2, C_3, z_1, z_2, z_3)$ exactly two of the operators, C_i, will be velocity operators, the third is $\mathcal{K}^m$. The purpose of this section is to show that for each term in Eqs. (39) the vertex corrections vanish so that the appropriate I is given simply by

$$I^{(2)}(C_1, C_2; z_1, z_2) = \mathrm{Tr} C_1 \bar{G}(z_1) C_2 \bar{G}(z_2) \tag{61a}$$

and

$$I^{(3)}(C_1, C_2, C_3; z_1, z_2, z_3) = \mathrm{Tr} C_1 \bar{G}(z_1) C_2 \bar{G}(z_2) C_3 \bar{G}(z_3) \ . \tag{61b}$$

Each $I^{(2)}$ listed in Eqs. (39) can be handled easily. Using the cyclic property of $I^{(2)}$ discussed in Ref. 4, it will be sufficient to show $\Gamma_n^{(2)}(v) = 0$. To see that $\Gamma_n^{(2)}(v)$ vanishes we substitute Eq. (48) into (52a). It follows then that each term in Eq. (52a) involves $\langle n | \bar{G} v \bar{G} | n \rangle$. Then it can be seen that $\Gamma_n^{(2)}(v)$ is proportional to $\langle n | \bar{G} v \bar{G} | n \rangle$ and vanishes because

$$\langle n | \bar{G} v \bar{G} | n \rangle = \langle 0 | \bar{G} v \bar{G} | 0 \rangle = 0 \ ,$$

since the velocity operator v is odd under parity transformation and $\bar{G}$ is even.

To show that the vertex correction in $I^{(3)}(v_x, \mathcal{K}^m, v_y)$ vanish, we use two facts. The first is that $\Gamma_n^{(2)}(v) = 0$. This eliminates all diagrams on the right-hand side in Fig. 3(a), except the first, second, fifth, and eleventh. The second and eleventh diagrams are, respectively, given by $\mathrm{Tr}[C_1 \bar{G} \times \langle T_n \bar{G} C_2 \bar{G} T_n \bar{G} C_3 \bar{G} T_n \rangle \bar{G}]$ and Eq. (54c) with C_1, C_2, C_3 equal, respectively, to $v_x, \mathcal{K}^m, v_y$. They vanish because they also involve $T_n \bar{G} v \bar{G} T_n$ which, using Eq. (48a), is proportional to $\langle n | \bar{G} v \bar{G} | n \rangle = 0$. The fifth diagram contains $\Gamma_n^{(2)}(\mathcal{K}^m)$ which is not zero. But this diagram is just that in Fig. 2(a) with C_1, C_2, C_3 replaced by $v_x, \mathcal{K}^m, v_y$, respectively. The appropriate analytical expression, from (54a), is therefore

$$\sum_n \mathrm{Tr} v_x \bar{G} \Gamma_n^{(2)}(\mathcal{K}^m) \bar{G} v_y \bar{G}$$

which vanishes, because the trace when evaluated in the Bloch basis $|k\rangle$ becomes proportional to

$$\sum_n \langle n | \Gamma_n^{(2)} | n \rangle \sum_k v_x(k) \bar{G}(k) v_y(k) \bar{G}(k) = 0 \ .$$

Similar arguments hold for $I^{(3)}(v_x, v_y, \mathcal{K}^m)$. Equations (61) thus follow.[18]

V. DISCUSSION AND NUMERICAL EXAMPLES

Using the results of the decoupling schemes of Sec. IV and evaluating the integrals in Eqs. (39a) and (39b) as outlined in Appendix B, the configuration-averaged conductivities, the Hall coefficient at zero temperature, and the thermoelectric power at low temperatures can be obtained from

$$\sigma \equiv \langle L_{EE}^{xx} \rangle = (n_{\mathrm{eff}} e^2/m)(2\Delta)^{-1} \ , \tag{62a}$$

$$\langle L_{EE}^{xy}(H) \rangle = \omega_c (2\Delta)^{-1} [(n_{\mathrm{eff}}^H e^2/m)(2\Delta)^{-1}] \ , \tag{62b}$$

and

$$\langle R_H \rangle = (ec)^{-1} n_{\mathrm{eff}}^H / (n_{\mathrm{eff}})^2 \tag{62c}$$

and Eq. (33) for Q. Here $\Delta = |\mathrm{Im}\Sigma(E_F)|$, where Σ is defined in Eq. (49). The expression for σ is identical to that found in Ref. 4. The quantities n_{eff} and n_{eff}^H are defined by

$$\frac{n_{\mathrm{eff}}}{m} = 1 - \Delta \frac{\partial}{\partial \Delta} \mathrm{Im}\Phi^{xx}[E_F - \mathrm{Re}\Sigma(E_F) - i\Delta(E_F)] \tag{63a}$$

and

$$\frac{n_{\mathrm{eff}}^H}{m} = \left(1 - \Delta \frac{\partial}{\partial \Delta} - \frac{\Delta^2 \partial^2}{3 \partial E_F^2}\right) \times \mathrm{Im}\Psi^{xy}[E_F - \mathrm{Re}\Sigma\ (E_F) - i\Delta(E_F)] \ , \tag{63b}$$

where

$$\Phi^{xx}(z) = \pi^{-1} \int d\xi (z - \xi)^{-1} \int d^3k \times (2\pi)^{-3} [v_x(k)]^2 \delta[\xi - W(k)] \ , \tag{64a}$$

$$\Psi^{xy}(z) = m\pi^{-1} \int d\xi (z - \xi)^{-1} \int d^3k \times (2\pi)^{-3} [v_y(k)]^2 M^{-1}{}_{xx}(k) \delta[\xi - W(k)] \ . \tag{64b}$$

Here ω_c is the free-electron cyclotron frequency eH/mc, $W(k)$ is the energy wave-number dispersion relation for the simple cubic tight-binding crystal, Eq. (5), and c is the velocity of light.

In the rigid-band limit, $\delta \ll 1$, which will be of interest for comparison purposes,

$$\Sigma(z) = \epsilon + xy\delta^2 F(z - \epsilon) \ . \tag{65a}$$

The parameters of this equation were defined following Eq. (49). $F(E)$ is simply related to the density of states per atom in the pure crystal $g(E)$ by

$$-\pi^{-1}\, \mathrm{Im}F(E + i0) = g(E) \ . \tag{65b}$$

The Fermi energy for a given alloy, which plays an important role in the transport coefficients, can be expressed in terms of the electron concentration per atom c by means of the relationship

$$c = -\pi^{-1} \int_{-\infty}^{E_F} dE\, \mathrm{Im} F[E - \Sigma(E)] \ . \tag{66}$$

Here the symbol c should not be confused with the other traditional use of c as the velocity of light. Because the CPA is inadequate at the band edges,[1]

we shall consider only the case where the Fermi level is sufficiently far removed from the edges that the carrier concentration is in the metallic range.

Equations (62a) and (62b) are similar in form to analogous expressions for the transport coefficients resulting from the Boltzmann equation,[9] when the identification with the relaxation time $\tau=[2\Delta(E_F)]^{-1}$ is made. The reason for this simple result which involves only the imaginary part of the single-particle self-energy is that the vertex corrections vanish. Physically, this follows from the fact that there is no backscattering term in the Boltzmann equation and is a consequence of our assumption that the scattering is of short range only and therefore isotropic.

The quantities n_{eff} and n_{eff}^H play the role of the effective number of carriers in the transport coefficients. From Eqs. (63) and (64), it is easily seen that they depend in complicated but different ways on the pure crystal band shape as well as on the self-energy Σ. Furthermore, Eqs. (63) demonstrate that they both depend on the imaginary part of the self-energy Δ only to order Δ^2 and higher. For all alloy parameters considered here $\Delta^2 < |\mathrm{Re}\Sigma|$ where Δ and Σ are dimensionless, and consequently the dependence of n_{eff} and n_{eff}^H on Δ will be neglected. This implies that the only effect of alloying on n_{eff} and n_{eff}^H for the cases of interest here is to shift the energy of an electron at the Fermi surface by an amount $-\mathrm{Re}\Sigma(E_F)$.

Following Koster and Slater,[19] the expressions for n_{eff} and n_{eff}^H may be reduced to single integrals involving Bessel functions for the case of the simple cubic tight-binding band. The Fermi energy dependence of n_{eff} and n_{eff}^H is given by

$$n_{eff} \propto \int_0^\infty dt \cos[E_F - \mathrm{Re}\Sigma(E_F)]t[J_0(t)+J_2(t)]J_0^2(t)\,, \tag{67a}$$

$$n_{eff}^H \propto -\int_0^\infty dt \sin[E_F - \mathrm{Re}\Sigma(E_F)]t[J_0(t)+J_2(t)]J_0(t)J_1(t)\,. \tag{67b}$$

These integrals have been tabulated.[20]

The remainder of this section will be devoted to evaluating transport coefficients for various alloy parameters x, δ, and c. Section V A will discuss the behavior of σ, Q, and R_H as functions of the Fermi energy E_F for several choices of x and δ. Section V B will contain a discussion of these coefficients as functions of x when c and δ are held fixed.

This latter case clearly corresponds more closely to what is observed experimentally. An isolectronic alloy with two fixed components A and B has constant electron concentration c per atom and a fixed scattering strength parameter δ independent of the relative proportions of the two types of atoms.

Several general statements may be made about the parameters n_{eff}, n_{eff}^H, and $\Delta=(2\tau)^{-1}$ at the outset:

(i) σ varies at Δ^{-1} and therefore depends strongly on Δ.

(ii) Q, since it is a derivative of σ, will be even more sensitive to the behavior of Δ.

(iii) Because the scattering is isotropic, Δ drops out explicitly from the expression for the Hall coefficient. Furthermore, because n_{eff} and n_{eff}^H depend primarily on $\mathrm{Re}\Sigma$, the imaginary part of the self-energy does not contribute significantly to R_H [see Eq. (62c)].

A. Variations of Transport Coefficients with E_F for Fixed x and δ

Many of the results in this section and in Sec. V B will be compared to those of the rigid-band theory. Consequently, the behavior of the three transport coefficients and the subsidiary quantities Δ, n_{eff} and n_{eff}^H at small δ will be discussed first with emphasis on the role of critical points in the pure crystal band. To exhibit our results in the common units, we adopt a model crystal with a bandwidth of 10 eV and a unit-cell dimension $a=2$ Å.

Equation (65a) shows that the critical points appear in $\Delta=|\mathrm{Im}\Sigma|$. We shall now show that they also influence the behavior of σ and Q as functions of E_F. From Fig. 4(a) it is clear that $n_{eff}(E_F)$ is slowly varying with energy in the neighborhood of the critical points at $\pm\frac{1}{3}$ for the rigid-band case. By contrast, as will be shown shortly, just below the lowest critical-point energy Δ increases sharply. Therefore, σ which depends on $n_{eff}(E_F)/\Delta(E_F)$ must decrease rapidly. The other point at $+\frac{1}{3}$ will give rise to an analogous behavior.

These results are illustrated in Figs. 5(a) and 6(a). In Fig. 5(a), $\Delta/\Delta^{\max}$ is plotted in the rigid-band case. $\Delta^{\max}$ is the maximum value of Δ for given x and δ. Δ is proportional to the density of states $g(E)$ as seen in Eqs. (65). The critical points M_0, M_1, M_2, and M_3 are labeled on this curve and it is seen that Δ is zero for energies in units of half-bandwidth greater than $+1$ and less than -1. Figure 6(a) illustrates the role of critical points in the conductivity for the small $\delta \ll 1$ case. The first dip in σ is due to the critical point M_1, the second is due to M_2. The conductivity is appropriately zero at the band edges since the number of carriers vanishes there.

Because the thermoelectric power is the derivative of σ, the effects of critical points are even more pronounced in Q. It will change sign when the conductivity has a local maximum or minimum. It is clear from Fig. 6(a) that this occurs five times in the rigid-band case. Consequently, as shown in Fig. 7(a) these five extrema are evident in Q as five sign changes. Just as the two dips in σ were seen to arise from the critical points M_1 and M_2, four of

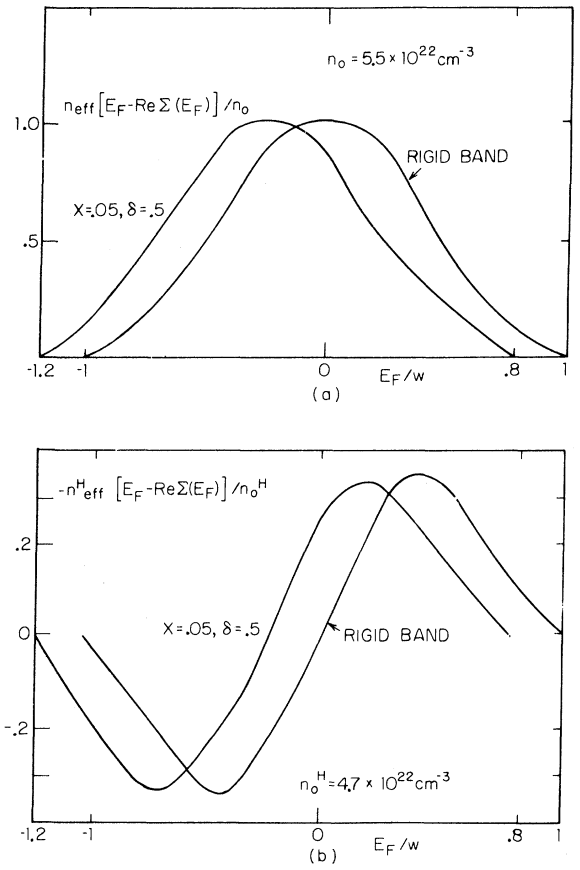

FIG. 4. Carrier densities for the (a) field-independent and (b) field-dependent conductivity versus E_F (in units of half-bandwidth) at $T=0$. The two curves in each figure correspond, respectively, to the rigid-band limit $\delta \ll 1$ and $x=0.5$ and to the case $\delta=0.5$, $x=0.05$. The model alloy adopted has bandwidth $2w=10$ eV and unit-cell dimension $a=2$ Å.

these sign changes may be seen to arise directly from them. As shown in the figure, the thermoelectric power is asymptotically $-\infty$ and $+\infty$ at the lower and upper band edges, respectively.

Because R_H is weakly dependent on Δ, the critical points in the pure crystal are not expected to influence the behavior of R_H appreciably. The Hall coefficient will change its sign when $E_F = \mathrm{Re}\Sigma$ and in the rigid-band limit this occurs at $E_F = \epsilon$. This is evident from the rigid-band curve in Fig. 4(b) which shows that $n^H_{eff}[E_F - \mathrm{Re}\Sigma(E_F)]$ is zero when its argument vanishes ($\mathrm{Re}\Sigma = \epsilon$ is chosen for simplicity to be zero in the rigid-band illustration). As shown in Fig. 8(a), R_H in comparison to Q behaves very simply in the case of $\delta \ll 1$. It changes sign once, as anticipated above, and it asymptotically approaches $-\infty$ and $+\infty$ at the band edges. It should be noted that in this special case Q also changes sign at ϵ which in our rigid-band example equals zero. But, comparing Fig. 7(a) and 8(a), it is clear that Q and R_H differ in sign for appreciable regions of E_F. Even in the case of very small δ the sign of the charge carriers are determined from the thermoelectric power and the Hall coefficient will not be the same except near the band midpoint and edges.

To discuss the coefficients for δ not small, the change in structure of n_{eff} and n^H_{eff} and Δ upon alloying must be investigated. Figures 4(a) and 4(b) show n_{eff} and n^H_{eff} for the rigid-band case and the case of moderately large δ (= 0.5). They demonstrate that, except for a shift along the energy axis, these functions do not change very much with increasing alloying. However, Figs. 5(a)–5(d) show that Δ does change appreciably. It is of interest in connection with Fig. 5 to compare the rigid-band behavior discussed above with that of $\delta = 0.05$ and $x = 0.1$ which presumably represents the case of weak scattering. It is somewhat surprising that the rigid-band description of the alloy is not applicable, for Δ is not proportional to the (symme-

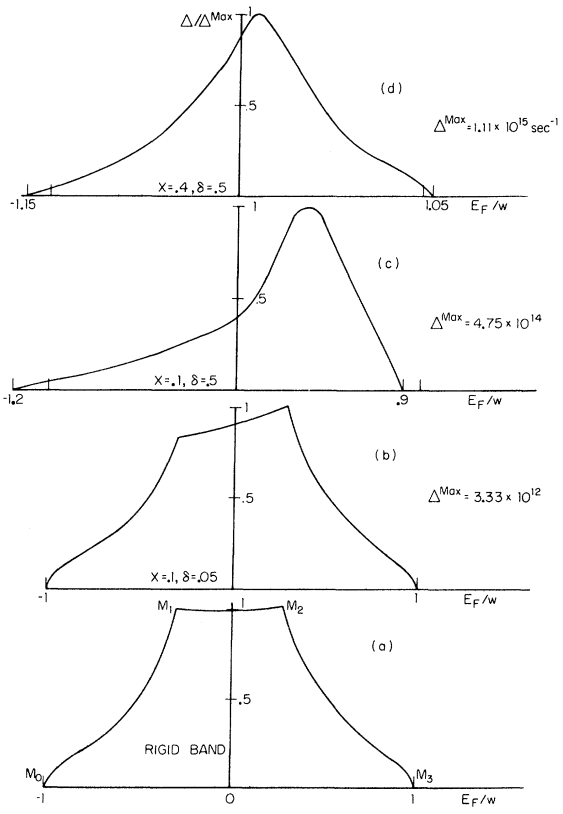

FIG. 5. Δ/Δ^{max} (proportional to the inverse relaxation time) versus E_F at $T=0$. (a) rigid-band limit; (b) scattering strength $\delta=0.05$ and impurity concentration $x=0.1$; (c) $\delta=0.5$, $x=0.1$; and (d) $\delta=0.5$, $x=0.4$.

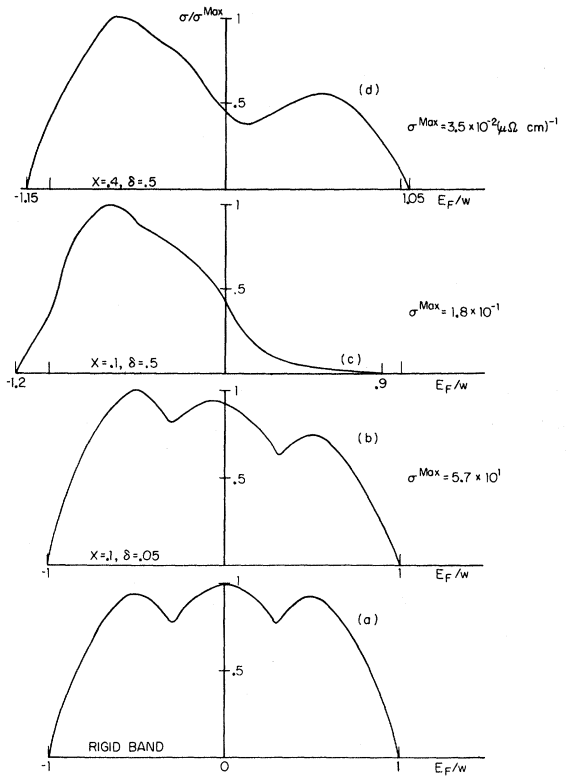

FIG. 6. Conductivity versus E_F for same four choices of (δ, x) as in Fig. 5. The two dips in Fig. 6(a) appear near critical-point energies and are washed out as δ increases.

tric) pure crystal density of states and therefore is not given by Eq. (65a) as Fig. 5(b) shows. The asymmetry which is apparent here is due to the fact that when $\delta > 0$, so that $\epsilon^A > \epsilon^B$, the impurity level lies in the top half of the band. This gives rise to increased damping of electrons whose energies are in this region. The critical points are still evident for this small δ and the bandwidth is not appreciably different from Fig. 5(a).

The sharp critical-point structure in Δ is no longer visible when δ is increased ten times to 0.5 but x is maintained at 0.1, as shown in Fig. 5(c). The damping is much more localized near the top of the band than in the previous case for the reason that the fairly strongly scattering impurity atomic energy level lies in this region. The band edges have shifted so that they lie at -1.2 and 0.9 and the magnitude of Δ has increased by a factor of 100.

Now, to compare the results obtained with the same δ but different x, we refer to Figs. 5(c) and 5(d). In Fig. 5(d) Δ is plotted for $x = 0.4$, $\delta = 0.5$. It is seen that the damping is no longer localized in the top half of the band when x is increased from 0.1 to 0.4. This is clearly not to be associated with a shift in the impurity atomic energy level ($\epsilon^A = \frac{1}{2}\delta$) since δ is constant in Figs. 5(d) and 5(c). Instead it is associated with the fact that as x increases from 0.1 to 0.4, the density of states nearer to the middle of the band rises,[21] thus causing the damping to increase in this energy region.

After having discussed the basic quantities n_{eff} and n^H_{eff}, and Δ for general alloy parameters and the transport coefficients in the rigid-band limit, we next focus attention on the three transport coefficients for the more general case. It was seen in Fig. 4 that n_{eff} and n^H_{eff} change little with alloying; consequently, one expects that the structural changes in σ will be due primarily to Δ. Therefore, Figs. 6(b)–6(d) which show σ versus E_F can be almost entirely explained in terms of Figs. 5(b)–5(d) which plot Δ versus E_F.

Figure 6(b) shows that for $\delta = 0.05$, $x = 0.1$, the conductivity reflects the asymmetry in Δ becoming smaller in the top half of the band where Δ is large relative to its value in the lower half. The critical points are still evident in σ at $\delta = 0.05$. In Fig. 6(c) for $\delta = 0.5$, $x = 0.1$ just as in Fig. 5(c), the critical points no longer appear and the conductivity has decreased in magnitude by a factor of several hundred

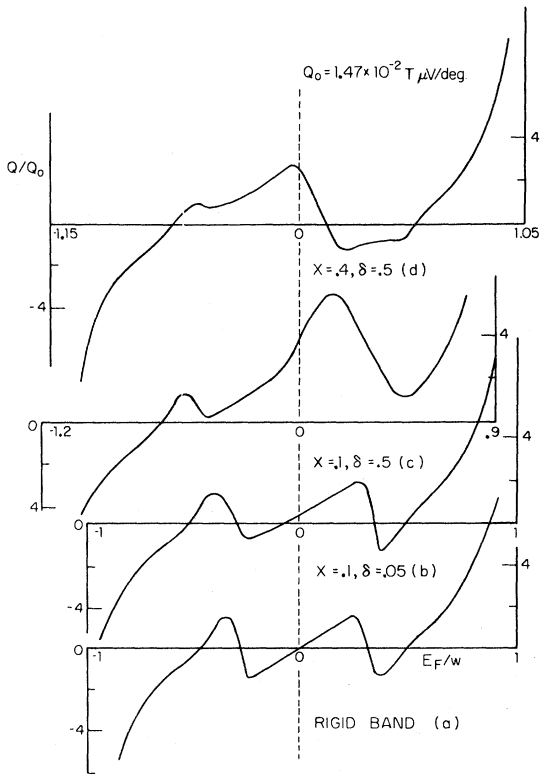

FIG. 7. Thermoelectric power Q versus E_F for the same four choices of (δ, x) as in Figs. 5 and 6. The upper and lower band edges are indicated by vertical lines at which Q approaches $+\infty$ and $-\infty$, respectively.

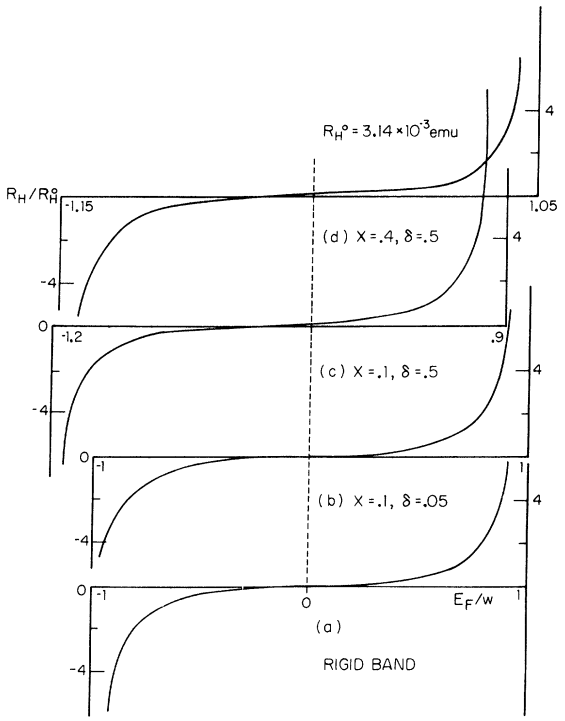

FIG. 8. Hall coefficient versus E_F for same alloy parameters as in Figs. 5–7. The upper and lower band edges are indicated by vertical lines at which R_H approaches $+\infty$ and $-\infty$, respectively.

from the previous case. The effects of increasing x for fixed δ are quite pronounced as seen by comparing Figs. 6(c) and 6(d) in which δ is fixed at 0.5 and x changes from 0.1 to 0.4. The maximum in Δ in Fig. 5(d) is reflected as a minimum in σ for the latter case. It occurs because Δ has a maximum in an energy region where n_{eff} is not inappreciable. By contrast, for the smaller $x = 0.1$, the energy of highest damping occurs too near the top of the band, where n_{eff} is very small, to be apparent as a minimum in the conductivity.

The thermoelectric power (TEP), because it is a derivative of $\ln\sigma$ can be easily interpreted from the previous discussion. Increasing δ from the rigid-band value [Fig. 7(a)] to 0.05 and keeping x fixed at 0.1 does not noticeably alter the shape of the Q-versus-E_F curve except to change the position of each of the five zeros as shown in Fig. 7(b). Upon again increasing δ to 0.5, for fixed $x = 0.1$, Q changes appreciably and crosses the energy axis only once, reflecting the single extremum in the conductivity [Fig. 6(c)] as shown in Fig. 7(c). However, the small dips in Q indicate that residual critical-point behavior is present even for this rather large δ. As x increases from 0.1 to 0.4 and δ remains equal to 0.5, the minimum which appears in the conductivity [Fig. 6(d)] is reflected as a sign change in Q as Fig. 7(d) shows.

It is clear from Figs. 7 that the TEP is extremely sensitive to changes in the band structure due to alloying. As Fig. 8 shows, R_H is not nearly as sensitive. Furthermore, its behavior as a function of E_F in the rigid-band limit is simple compared with that of Q [see Figs. 7(a) and 8(a)].

A comparison of Figs. 8 and 7 illustrates the following general properties of the two transport coefficients as functions of E_F. The Hall coefficient and the TEP do not have the same sign except in the upper and lower regions of the band when both asymptotically approach $+\infty$ and $-\infty$ correspondingly. In this region, the effective-mass approximation may be used to determine the sign of Q and R_H. The TEP reflects critical points and changes in the imaginary part of the self-energy; the Hall coefficient does not. The primary effect of alloying on the latter quantity is to shift the energy at which R_H changes sign by an amount $-\mathrm{Re}\Sigma(E_F)+\epsilon$. This shift, although not very big, corresponds physically to the fact that the "carrier sign" changes when the symmetric band is not exactly half-full. For example, at $\delta = 0.5$, $x = 0.1$, the electron concentration per atom c, at which the sign of the charge carriers is reversed occurs at $c = 0.49$.

B. Variations of the Transport Coefficients with x for Fixed c and δ

Section V A discussed the behavior upon alloying of the three transport coefficients as the Fermi energy was continuously varied. In this section we shall fix the electron concentration c and allow x, the impurity concentration, to vary continuously; using Eq. (66), the Fermi energy may be determined in terms of c, δ, and x for each point x. In contrast to the previous section, the results obtained here, although more relevant to experiment, are fairly complicated to interpret. They depend on the variation in E_F with x for fixed c as well as on the behavior of the coefficients as functions of E_F for fixed x as discussed in Sec. V A.

Two curves of E_F versus x for $\delta = 0.5$, $c = 0.2$, and $\delta = 0.5$, $c = 0.5$ are plotted in Figs. 9(a) and 9(b). Also shown are the straight lines which would be obtained if the Fermi energy were computed in the rigid-band limit as the average of the Fermi energies of the two components in their respective pure crystals. The end points $x = 0$, $x = 1$ of the curves of E_F versus x must coincide with those of the straight line. At $\delta = 0.5$, Fig. 9 show that departures from rigid-band behavior are signigicant. For $c = 0.5$, the Fermi energy is antisymmetric about $x = 0.5$ as expected from our assumption that the pure crystal band density of states $g(E)$ is symmetric about the band midpoint. The

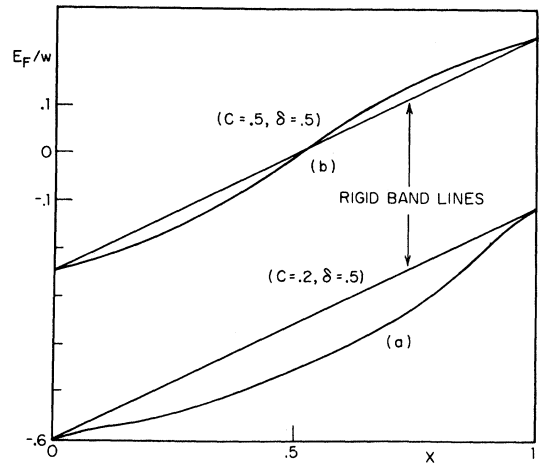

FIG. 9. E_F in units of half-bandwidth versus x for $\delta = 0.5$ and two electron concentrations per atom, $c = 0.2$ [Fig. 9(a)] and $c = 0.5$ [Fig. 9(b)]. The straight lines are the rigid-band limits.

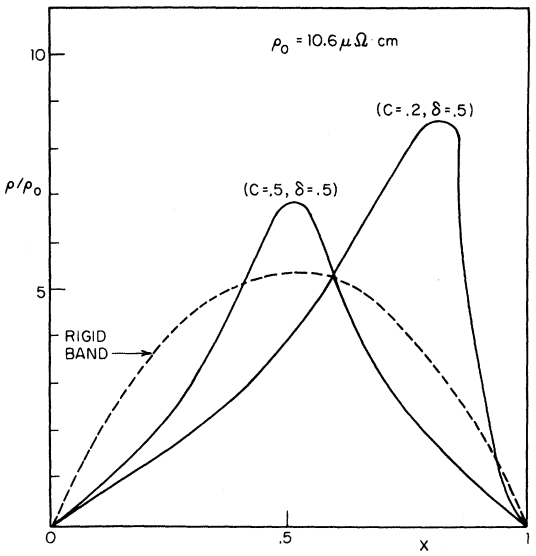

FIG. 10. Resistivity versus x for $\delta = 0.5$. Dotted line is Nordheim $x(1-x)$ approximation. Solid curves refer to CPA results for electron concentrations per atom of $c = 0.2$ and $c = 0.5$.

detailed behavior of these curves can be understood by looking at the function $F[E - \Sigma(E)]$ [see Eq. (66)] which will not be discussed here.[21]

As in Sec. V A, it will be convenient to refer the x-dependent behavior of the coefficients to the weak-scattering limit. The discussion will be limited to R_H and σ since Q can be determined from σ and the functional dependence of E_F versus x. The resistivity ρ is given by the Nordheim[22] rule in this limit,

$$\rho \equiv \sigma^{-1} 2\pi x(1-x)\delta^2 g(E_F)/n_{\text{eff}}(E_F)e^2 m^{-1}. \qquad (68)$$

In this expression the x dependence of E_F is neglected for small δ, so that the resistivity varies as $x(1-x)$. Also for small δ,

$$ecR_H = n_{\text{eff}}^H[E_F(x) - \epsilon(x)]/n_{\text{eff}}^2[E_F(x) - \epsilon(x)]. \qquad (69)$$

Since $E_F(x) - \epsilon(x)$ is x independent in the rigid-band limit R_H is also.

If δ is then increased to moderate values, the x dependence of the two transport coefficients is no longer simple. Figure 10 shows the resistivity for $c = 0.2$ and 0.5 and $\delta = 0.5$. The dotted line is the Nordheim limit in the same units for this δ and $c = 0.5$. It is clearly not a good approximation to the resistivity. The most striking deviation from the rigid-band behavior for $c = 0.5$ is the sharp peak at $x = 0.5$. This is due to a minimum in the conductivity which appears for $\delta = 0.5$, $c = 0.5$ at this x. This minimum in σ like that shown in Fig. 6(d) occurs for values of x away from 0 and 1 and results, as discussed earlier, from the appearance of a maximum in the imaginary part of Σ, away from the band ends. For the electron concentration $c = 0.2$, the peak in the resistivity appears at $x \cong 0$. Its origin is the same as that discussed in connection with Fig. 6(d). This curve is clearly not symmetric about $x = 0.5$ as the Nordheim rule suggests. As in Sec. V A, Δ plays an important part in determining the behavior of σ.

The Hall coefficient, on the other hand, reflects the behavior of $\text{Re}(\Sigma)$. Figures 11(a) and 11(b) show the x dependence of $E_F - \text{Re}\Sigma(E_F)$. While the

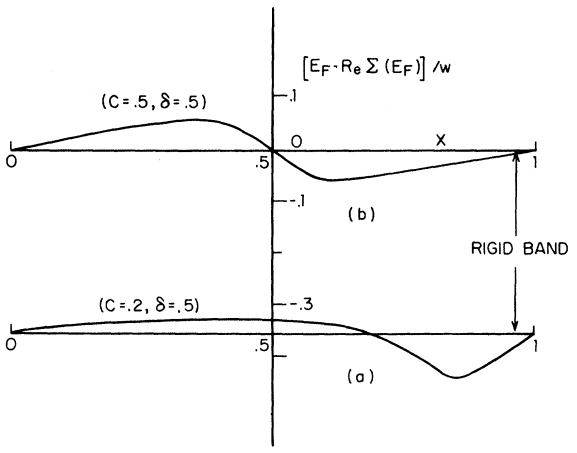

FIG. 11. $E_F - \text{Re}\Sigma(E_F)$ versus x in units of half-bandwidth for $c = 0.2$ [Fig. 11(a)] and $c = 0.5$ [Fig. 11(b)]. The scattering strength δ is 0.5. The rigid-band horizontal lines are indicated by arrows.

curve for $c = 0.5$ is antisymmetric about $x = 0.5$ for the symmetric density of states, that for $c = 0.2$ is not. The straight lines shown are the rigid-band approximations to this function. Deviations from the lines are significant. Using Figs. 11, Eq. (62c), and the rigid-band curves in Fig. 4, it is possible to predict the x-dependent behavior of R_H. The sign of R_H and its zero coincide with that of $(E_F - \mathrm{Re}\Sigma)$. Figure 12(a) shows R_H versus x for $c = 0.2$. Figure 12(b) shows the curve for $c = 0.5$. The straight lines are the rigid-band limits. The behavior of $E_F - \mathrm{Re}\Sigma(E_F)$ of Fig. 11 is clearly mirrored in that of the Hall coefficient shown in Fig. 12.

ACKNOWLEDGMENT

The authors are grateful to Dr. E. S. Kirkpatrick whose suggestions concerning the numerical aspects of this problem were extremely helpful.

APPENDIX A: SOME PROPERTIES OF RESPONSE FUNCTIONS

We define the correlation function χ for electrons in an alloy by

$$\chi(\alpha,\beta;z) \equiv \chi_{\alpha\beta}(0,z) = \chi'_{\alpha\beta}(0,z) + i\chi''_{\alpha\beta}(0,z), \tag{A1}$$

where

$$\chi'(0,z) = \pi^{-1}\mathcal{P}\int d\omega' \frac{\chi''(0,\omega')}{(\omega'-z)} \quad . \tag{A2}$$

Here z is a complex frequency and χ is a tensor quantity. χ'' is defined in Eq. (20). We now list certain properties of χ and $\chi(H)$.[13] This last function is the correlation function in the presence of an external magnetic field treated linearly. Statements which are confined to χ_{JJ} may be extended to χ^q_{JJ}:

(i) $\chi''_{JJ}(0,\omega)$ is real and odd in ω.

(ii) $\chi''_{JJ}(0,\omega;H)$ is imaginary and even in ω.

(iii) From (A2) the evenness and oddness properties of χ' and χ'' are reversed.

(iv) Including a damping mechanism enables one to go smoothly to the $\omega = 0$ limits of

$$L_{EE}(\omega) = (\pi i)^{-1}\int_{-\infty}^{\infty} d\omega' \frac{\chi''_{JJ}(\omega')}{\omega'(\omega'-\omega-i0)} \quad .$$

Therefore

$$\mathrm{Im}L^{ii}_{EE}(0,\omega)\big|_{\omega=0} = 0 \tag{A3}$$

and

$$\mathrm{Im}L^{xy}_{EE}(0,\omega;H)\big|_{\omega=0} = 0 \tag{A4}$$

because both these functions are odd.

(v) Using time-reversal invariance, it follows that

$$\chi''^{ij}_{JJ}(0,\omega) = \chi''^{ji}_{JJ}(0,\omega) \tag{A5}$$

and

$$-\chi''^{ji}_{JJ}(0,\omega;H) = \chi''^{ij}_{JJ}(0,\omega;H) \quad . \tag{A6}$$

For C_1, C_2 arbitrary we have

(vi) $$\chi(C_1,C_2;z) = \chi^*(C_1,C_2;-z^*), \tag{A7}$$

(vii) $$\chi(\mathcal{O}C_1\mathcal{O}^\dagger, \mathcal{O}C_2\mathcal{O}^\dagger; z; \mathcal{O}C_3\mathcal{O}^\dagger) = \chi(C_1,C_2;z;C_3), \tag{A8}$$

where $\mathcal{O}$ is any translation operator of the pure crystal symmetry group. It is assumed here that χ is the exact *configuration-averaged* response function for the random alloy in the presence of an external field C_3. (The configuration average restores the lattice symmetry.) This equation is valid to all orders in C_3,

(vii) $$\lim_{z\to\infty}\chi(C_1,C_2;z) = z^{-1}\langle[C_1,C_2]\rangle_T \quad , \tag{A9}$$

where the subscript T denotes a thermal average.

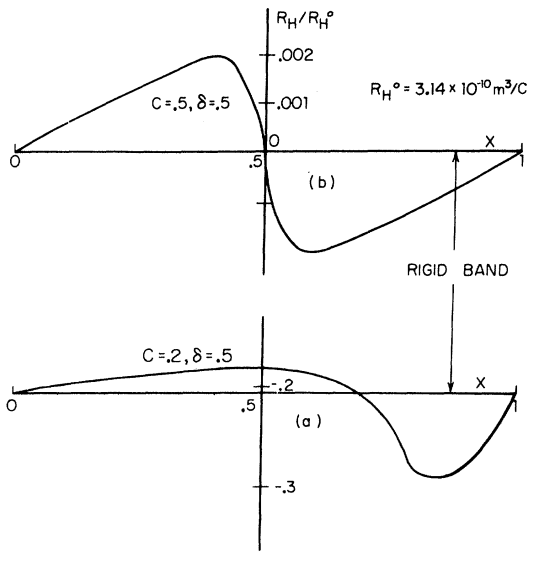

FIG. 12. Hall coefficient versus x for same alloy parameters as in Fig. 11. Straight lines are rigid-band limits.

APPENDIX B: EVALUATION OF $\langle L^{xy}_{EE}(H)\rangle$ AND $\langle L^{xx}_{EE}\rangle$

In this section we briefly outline the manipulations involved in evaluating Eqs. (39a)[4] and (39b).[21] Because the vertex corrections were shown to vanish for each $I^{(3)}$ and each $I^{(2)}$ in these equations, the problem of calculating $\langle L^{xy}_{EE}(H)\rangle$ and $\langle L^{xx}_{EE}\rangle$ is reduced to treating a system of damped electrons in a periodic crystal with Green's function $\bar{G}(z) = [z - W - \Sigma(z)]^{-1}$, where W is the pure crystal Hamiltonian given by Eq. (5) and Σ is defined in Eq. (49).

To obtain $\langle L^{xy}_{EE}(H)\rangle$ we proceed in three stages. *First*, we evaluate explicitly

$$I^{(3)}(v_x, \mathcal{K}^m, v_y) = \sum_{RR'} v_x\left(\frac{\nabla_R}{i}\right)(\overline{G}\mathcal{K}^m\overline{G})_{RR'}v_y\left(\frac{\nabla_{R'}}{i}\right)\overline{G}_{R'R}$$

and

$$I^{(3)}(v_x, v_y, \mathcal{K}^m) \ .$$

These expressions involve $(\overline{G}\mathcal{K}^m\overline{G})_{RR'}$ which has been determined for free electrons.[23] We extend the arguments of Ref. 23 to calculate the field-dependent Green's function for electrons in a crystal. *Second*, we combine the I's in Eq. (39b) and evaluate

$$\begin{aligned} I^{\text{tot}} \equiv & I^{(3)}(v_x, \mathcal{K}^m, v_y) + I^{(3)}(v_x, v_y, \mathcal{K}^m) \\ & + I^{(2)}(v_x - eA_y M^{-1}{}_{yy}/c) + I^{(2)} \\ & \times(-eA_x M^{-1}_{xx}/c, v_y) \end{aligned} \tag{B1}$$

in the crystal coordinate representaion. It is seen that Block transforms of I^{tot} may be simply evaluated since I^{tot} is a sum of translationally invariant quantities. *Third*, we perform the λ summations and the ω' and η integrations implied by (39b). At the end of the discussion of $\langle L^{xy}_{EE}(H)\rangle$, we shall briefly sketch the calculation of $\langle L^{xx}_{EE}\rangle$ which is considerably simpler.

To evaluate $I^{(3)}(v_x, \mathcal{K}^m, v_y)$ we first consider

$$G^{(H)} = \overline{G} + \overline{G}\,\mathcal{K}^m G^{(H)} = \overline{G} + \overline{G}\,\mathcal{K}^m\,\overline{G} + \mathcal{O}(H^2) \ . \tag{B2}$$

$G^{(H)}$ can be expanded in a power series in H. Following Ref. 23 we write

$$G^{(H)}_{RR'} \equiv \exp(-ie\vec{\mathrm{H}}\cdot\vec{\mathrm{R}}\times\vec{\mathrm{R}}'/2c)(\overline{G} + \hat{G}_1 + \hat{G}_2 + \cdots)_{RR'} \ , \tag{B3}$$

where the subscripts RR' refer to matrix elements in Wannier space, and $\hat{G}_1$ is defined to be linear in H, $\hat{G}_2$ quadratic, etc. From Eq. (B2), it follows that

$$\begin{aligned} \exp\left(\frac{-ie\vec{\mathrm{H}}\cdot\vec{\mathrm{R}}\times\vec{\mathrm{R}}'}{2c}\right)\left\{\left(E - \Sigma(E) + \frac{e\vec{A}(R)\cdot\vec{v}(\nabla_R/i)}{c}\right)\overline{G}(E)_{RR'} + \left[E - \Sigma(E) - W\left(\frac{\nabla_R}{i}\right)\right]\hat{G}_1(E)_{RR'} + \mathcal{O}(H^2)\right. \\ \left. - \left[W\left(\frac{\nabla_R}{i}\right)\exp\left(\frac{-ie\vec{\mathrm{H}}\cdot\vec{\mathrm{R}}\times\vec{\mathrm{R}}'}{2c}\right)\right]\overline{G}(E)_{RR'} = \delta(R - R') \ . \end{aligned} \tag{B4}$$

We obtain from (B4) that

$$\begin{aligned} & -(e/2c)(\vec{\mathrm{R}} - \vec{\mathrm{R}}')\times\vec{\mathrm{H}}\cdot\vec{v}(\nabla_R/i)\overline{G}(E)_{RR'} \\ & \quad = [E - W - \Sigma(E)]\hat{G}_1(E)_{RR'} \end{aligned} \tag{B5a}$$

This equation is satisfied if

$$\hat{G}_1(E)_{RR'} = 0 \ . \tag{B5b}$$

To obtain (B5a) we have substituted $A(R) = \frac{1}{2}\vec{\mathrm{H}}\times\vec{\mathrm{R}}$ into (B4) and equated terms linear in H. Equation (B5b) follows by taking Bloch transforms of (B5a). The left-hand side of (B5a) involves

$$\sum_k \vec{v}(k)\times\vec{v}(k) = 0,$$

since $\nabla_k\overline{G}(E)_k \propto \vec{v}(k)$. Thus, from (B5b),

$$G^{(H)}_{RR'} = \exp\left(\frac{-ie\vec{\mathrm{H}}\cdot\vec{\mathrm{R}}\times\vec{\mathrm{R}}'}{2c}\right)[\overline{G}_{RR'} + \mathcal{O}(H^2)] \ . \tag{B6}$$

We next evaluate I^{tot} [Eq. (B1)]. If we consider only terms linear in H, the following equation is valid:

$$I^{(3)}(v_x, \mathcal{K}^m, v_y) + I^{(3)}(v_x, v_y, \mathcal{K}^m) = \mathrm{Tr}\, v_x G^{(H)} v_y G^{(H)} . \tag{B7}$$

Using (B6),

$$\begin{aligned} v_x\left(\frac{\nabla_R}{i}\right)G^{(H)}_{RR'} = & \exp\left(\frac{-ie\vec{\mathrm{H}}\cdot\vec{\mathrm{R}}\times\vec{\mathrm{R}}'}{2c}\right) \\ & \times\left\{\frac{-e(\vec{\mathrm{R}}'\times\vec{\mathrm{M}})_x}{2c}\ M^{-1}_{xx}\ \frac{\nabla_R}{i}\right\}\overline{G}_{RR'} + \mathcal{O}(H^2) \end{aligned} \tag{B8}$$

A similar equation may be written for $v_y G^{(H)}$. Then, using (B1), (B8), and the definition of $I^{(2)}$ [Eq. (40a)],

$$\begin{aligned} I^{\text{tot}} = & \sum_{RR'}\left(\frac{eH}{2c}\right)(R_y - R'_y)M^{-1}{}_{xx}\left(\frac{\nabla_R}{i}\right)\overline{G}_{RR'}v_y\left(\frac{\nabla_{R'}}{i}\right)\overline{G}_{R'R} - \sum_{RR'}\left(\frac{eH}{2c}\right)v_x\left(\frac{\nabla_{R'}}{i}\right) \\ & \times\overline{G}_{R'R}(R_x - R'_x)M^{-1}{}_{yy}\left(\frac{\nabla_R}{i}\right)\overline{G}_{RR'} \ . \end{aligned} \tag{B9}$$

Taking Bloch transforms of I^{tot}, inserting the energy arguments as in Eq. (39b), and performing the λ summations, one obtains

$$\langle L^{xy}_{EE}(H)\rangle = e^3H(\pi^2c)^{-1}\mathcal{P}\int\int d\omega'\,d\eta\left\{[o(\eta) - o(\eta+\omega')](\omega')^{-2}\sum_k M^{-1}{}_{xx}(k)v_y^2(k)\overline{G}_k''(\eta+\omega')\frac{\partial}{\partial\eta}\overline{G}_k''(\eta)\right\} \tag{B10}$$

after some manipulations. Here

$$\bar{G}_k''(\eta) = \mathrm{Im}[\eta - \Sigma'(\eta) + i\Delta(\eta) - W(k)]^{-1} = \mathrm{Im}\bar{G}_k(\eta) \ ,$$

where $\Sigma' = \mathrm{Re}\Sigma$ and $\Delta = |\mathrm{Im}\Sigma|$.

We next do the integrations implied by (B10). Because $\bar{G}_k(\eta + \omega)$ is analytic in the upper half-plane and zero at $\omega = \infty$, [1]

$$\pi^{-1} \mathcal{P} \int_{-\infty}^{\infty} d\omega' \bar{G}_k''(\eta + \omega')(\omega')^{-2} = \frac{\partial}{\partial \eta} \mathrm{Re}\bar{G}_k(\eta) \ . \quad \text{(B11)}$$

This identity can be used to perform the ω' integration. The η integration in (B10) is carried out by writing the integrand in terms of $\rho'(\eta) = -\delta(\eta - E_F)$. Equation (62b) then follows.

To evaluate $\langle L_{EE}^{xx} \rangle$, we use the results of the decoupling, the expression for $\bar{G}_k''(\eta)$ given following (B10), and the fact that $\rho'(\eta) = -\delta(\eta - E_F)$ at $T = 0$. Equation (62a) follows after some simple manipulations. [4]

Additional details of these somewhat lengthy calculations will be presented in Ref. 21.

---

*Work supported in part by Grant No. GP-8019 of the National Science Foundation and the Advanced Research Projects Agency.

†Present address: Institute of Solid State Physics, Czechoslovak Academy of Sciences, Prague, Czechoslovakia.

[1]B. Velický, S. Kirkpatrick, and H. Ehrenreich, Phys. Rev. 175, 747 (1968).

[2]P. Soven, Phys. Rev. 156, 809 (1967).

[3]P. Soven, Phys. Rev. 178, 1138 (1969).

[4]B. Velický, Phys. Rev. 184, 614 (1969).

[5]K. Liebermann Levin, B. Velický, and H. Ehrenreich, Bull. Am. Phys. Soc. 14, 320 (1968).

[6]E. Verboven, Physica 26, 1091 (1960).

[7]R. Kubo, J. Phys. Soc. Japan 12, 570 (1957); R. Kubo, S. Miyake, and N. Hashitsume, *Solid State Physics*, Vol. 17, edited by F. Seitz and D. Turnbull (Academic, New York, 1965).

[8]N. F. Mott and H. Jones, *The Theory of the Properties of Metals and Alloys* (Dover, New York, 1958) Chaps. VII and II.

[9]J. M. Ziman, *Electrons and Phonons* (Clarendon, Oxford, England, 1960) Chaps. VII, IX, and XII.

[10]J. P. Jan, in *Solid State Physics*, Vol. 5, edited by F. Seitz and D. Turnbull (Academic, New York, 1957).

[11]L. Onsager, Phys. Rev. 37, 405 (1931); 38, 2265 (1931).

[12]J. Friedel, Nuovo Cimento Suppl. 7, 287 (1958); E. Stern, Physics 1, 255 (1965).

[13]L. P. Kadanoff and P. C. Martin, Ann. Phys. (N. Y.) 24, 419 (1963).

[14]H. Ehrenreich, in *Proceedings of the International School of Physics "Enrico Fermi," Varenna*, 1966 (Academic, New York, 1966).

[15]The reader who is not interested in the theoretical details of the decoupling may skip Secs. III and IV and go directly to Sec. V which summarizes the results.

[16]We will frequently omit the arguments from $I^{(2)}(C_1, C_2; z_1, z_2)$, $I^{(3)}(C_1, C_2, C_3; z_1, z_2, z_3)$, $\bar{G}(z_i)$, and $T(z_i)$. These can easily be replaced using Eq. (50) as a model.

[17]It is not obvious from Fig. 3(a) that the three-particle vertex corrections depend only on C_2 and C_3. To justify writing Eq. (55), we must prove a "cyclic property" of $I^{(3)}$ which will be done below.

[18]Although the present paper is concerned with the vertex corrections to $I^{(3)}(v_i, \mathcal{K}^m, v_j)$ and $I^{(3)}(v_i, v_j, \mathcal{K}^m)$ for $i \neq j$, it can be shown that the vertex corrections to $I^{(3)}(v_i, \mathcal{K}^m, v_i)$ and $I^{(3)}(v_i, v_i, \mathcal{K}^m)$ also vanish.

[19]G. F. Koster and J. C. Slater, Phys. Rev. 96, 1208 (1954).

[20]T. Wolfram and J. Callaway, Phys. Rev. 130, 2207 (1963). We are grateful to Professor Callaway for providing us with additional numerical results not given in the reference.

[21]K. Levin, Ph. D. thesis, Harvard University, 1970 (unpublished).

[22]L. Nordheim, Ann. Physik 9, 607 (1931).

[23]D. Lynch, Ph. D. thesis, Harvard University, 1967 (unpublished); see also N. J. Horing, Ann. Phys. (N. Y.) 31, 1 (1965).